



Cite this: *Chem. Sci.*, 2024, **15**, 3140

All publication charges for this article have been paid for by the Royal Society of Chemistry

Received 30th November 2023
Accepted 9th January 2024

DOI: 10.1039/d3sc06425e
rsc.li/chemical-science

1 Introduction

In catalytic hydrogenation of both chemical transformations and biological functions, most of the hydrogen (H_2) activation processes occurred at the transition metal center.^{1–7} The exploration of metal-free systems for H_2 activation is quite appealing while rather challenging.⁸ Until 2006, Stephan and co-workers first reported one such unique system, the metal-free zwitterionic phosphoniumborate, which could reversibly activate H_2 under mild conditions. The proposed activation center of hydrogen was frustrated Lewis acid–base pairs (FLPs), which were defined as Lewis acids and bases sterically prevented from interaction to form Lewis acid–base adjuncts.⁹ Since then, the traditional paradigm of Lewis acid–base chemistry was changed and development of new FLPs for promoting

chemical reactivity was heatedly pursued.^{10–13} During the past few decades, a large number of homogeneous FLPs catalysts have been synthesized, which have found wide application in the fields of hydrogenation catalysis, small-molecule activation, organic chemistry, radical chemistry, transition metal chemistry, and enzyme models, as well as polymers and materials.^{14–16}

Despite the significant progress, the studies on heterogeneous (semi-solid and solid) FLPs catalysts were rather limited.^{17–30} The prominent examples included semi-solid (two-phase) FLPs catalysts of imine or nitrile modified gold nanoparticles,¹⁸ as well as solid FLPs catalysts that covered atypical oxides such as $In_2O_{3-x}(OH)_y$ and CeO_{2-x} .^{22,31} The abundant homogeneous while rare heterogeneous FLP catalysts indicated the difficulty in the design and preparation of heterogeneous FLP catalysts, which was attributed to the poor understanding of the structure–property relationship of solid FLPs. As such, the development of simple and practical synthetic strategies, detailed characterization of active sites, and insight into the reaction mechanism of heterogeneous FLPs are of high importance.

Among oxide supports used in industry, alumina is generally considered to be inert to H_2 and thus make no contribution to the hydrogenation process by supported metal catalysts. Close examination of the literature revealed that, however, alumina after dehydration treatment at 450–650 °C was able to hydrogenate ethylene, in which the active sites were believed to chemisorb and polymerize olefins on alumina.^{32,33} Nevertheless,

^aNew Cornerstone Science Laboratory, State Key Laboratory for Physical Chemistry of Solid Surfaces, Collaborative Innovation Center of Chemistry for Energy Materials, National & Local Joint Engineering Research Center of Preparation Technology of Nanomaterials, College of Chemistry and Chemical Engineering, Xiamen University, Xiamen 361005, China. E-mail: nfzheng@xmu.edu.cn; xdyi@xmu.edu.cn

^bInnovation Laboratory for Sciences and Technologies of Energy Materials of Fujian Province (IKKEM), Xiamen 361102, China

^cFujian Key Laboratory of Rare-Earth Functional Materials, Fujian Shanhai Collaborative Innovation Center of Rare-Earth Functional Materials, Longyan 366300, China

† Electronic supplementary information (ESI) available: Reagents, FTIR, TPD-MS, BET, XRD, HAADF-STEM, NMR, Fig. S1–S14 and Table S1. See DOI: <https://doi.org/10.1039/d3sc06425e>

‡ These authors contributed equally.



it remained elusive for the true active sites and the mechanism of the hydrogenation process.

Herein, we report the simple synthesis of a new type of pentacoordinated Al^{3+} -enriched Al_2O_3 , in which a large number of Lewis acidic and basic sites are co-present on the surface. The rigidity of the solid lattice prevents them from interacting to be acid–base adducts, thus giving access to heterogeneous FLPs catalysts. Interestingly, the as-obtained Al_2O_3 catalyst can activate hydrogen in the heterolytic pathway to produce equal amounts of $\text{O}-\text{H}^{\delta+}$ and $\text{Al}-\text{H}^{\delta-}$ in the absence of transition metals. The heterogeneous FLPs exhibited nice catalytic activity toward styrene hydrogenation in a stepwise mechanism.

2 Results and discussion

2.1 Preparation and characterization of the pentacoordinated Al^{3+} -enriched Al_2O_3 catalyst

The pentacoordinated Al^{3+} -enriched defective Al_2O_3 (denoted as d- Al_2O_3) catalyst was prepared by calcining aluminum hydroxide acetate, $[\text{Al}(\text{OH})(\text{CH}_3\text{COO})_2]$, at 500 °C in an inert atmosphere (N_2 or Ar). The catalyst was first characterized by solid state ^{27}Al magic-angle spinning nuclear magnetic resonance (^{27}Al MAS-NMR) spectroscopy (Fig. 1a).³⁴ Three peaks at chemical shifts of ~64, 33 and 6 ppm were assigned to Al^{3+} in tetrahedral (Al_t), pentahedral (Al_p) and octahedral (Al_o) coordination environments, respectively. Unexpectedly, a large proportion of Al_p was observed in the as-prepared d- Al_2O_3 ,³⁵ while only Al_t and Al_o were present in the lattice of commercial γ - Al_2O_3 (Fig. 1a).³⁶ As surface atoms play a key role in both substrate interaction and chemical transformation, we then

compared the relative content of surface Al_p by using gaseous Lewis base molecules of NH_3 .^{37–40} As shown in Fig. 1b, the coordination of NH_3 to surface Al_p led to a decrease in the intensity of the peak at ~33 ppm and correspondingly a distinct increase of the peak at ~6 ppm, suggesting the conversion of Al_p to Al_o after the treatment and thus the presence of rich Lewis acidic sites (Al_p) on the surface of d- Al_2O_3 .³⁶ The content of Al_p decreased from 39.1% in d- Al_2O_3 to 23.8% in NH_3 -d- Al_2O_3 (Fig. S1 and Table S1†). Thus, the portion of surface Al_p was estimated to be approximately 15.3% of the total Al^{3+} sites. The presence of surface Al_p on d- Al_2O_3 was also confirmed by *in situ* Fourier transform infrared spectroscopy of adsorbed NH_3 (*in situ* NH_3 -FTIR) and temperature-programmed desorption coupled with mass spectrometry using NH_3 (NH_3 -TPD-MS) (Fig. S2†). We also revealed that the d- Al_2O_3 surface featured richer and stronger Lewis basic sites than that of γ - Al_2O_3 by *in situ* CO_2 -FTIR and CO_2 -TPD-MS (Fig. S3†), although the specific surface area of γ - Al_2O_3 ($176 \text{ m}^2 \text{ g}^{-1}$) was higher than that of d- Al_2O_3 ($78 \text{ m}^2 \text{ g}^{-1}$) based on N_2 adsorption/desorption isotherms (Fig. S4†). With the Al_p sites serving as the Lewis acid sites and the surface oxygen species acting as the Lewis base sites, the rigid structure of d- Al_2O_3 prevented them from interacting to form acid–base adducts, so obtained d- Al_2O_3 was rich in FLPs. In addition, X-ray powder diffraction (XRD) characterization revealed that in comparison to well-crystallized γ - Al_2O_3 , d- Al_2O_3 was much less crystallized, indicating that Al^{3+} ions in the alumina lattice of d- Al_2O_3 were highly disordered and in diverse coordination modes (Fig. S5†).^{35,41} Aberration-corrected high-angle annular dark-field scanning transmission electron microscopy (HAADF-STEM) and fast Fourier transform (FFT) measurement also confirmed the amorphous characteristic of d- Al_2O_3 (Fig. S6†). These results match well with those of the solid state ^{27}Al MAS-NMR.

2.2 FLPs as active sites for the catalytic hydrogenation of styrene

With the presence of a large amount of FLPs on the as-obtained d- Al_2O_3 , we then employed the hydrogenation of styrene as a model reaction to demonstrate the surface reactivity of d- Al_2O_3 . 50 mg catalyst of d- Al_2O_3 and 20 μL styrene were added to 5 mL anhydrous toluene within a well-stirred autoclave, which was then charged with H_2 to 1 MPa and kept at 100 °C. As shown in Fig. 1c, d- Al_2O_3 exhibited nice reactivity toward hydrogenation, as ~100% styrene conversion was achieved within 4 h, and the complete conversion was confirmed using ^1H NMR spectra (Fig. S7†). Moreover, recycling tests revealed that the d- Al_2O_3 catalyst did not deactivate after 8 cycles, suggesting high robustness of FLP structures on the d- Al_2O_3 surface (Fig. S8†). We noted that the presence of FLPs on d- Al_2O_3 was the key to achieving the catalytic activity. In the control experiment where no catalyst was used or γ - Al_2O_3 without surface FLPs was employed, no reactivity was observed (Fig. 1d). In addition, we also used a gaseous probe to validate the necessity of FLPs for the hydrogenation. When NH_3 or CO_2 was used to neutralize surface Al_p or basic sites, the catalytic activity of the d- Al_2O_3 was significantly declined (Fig. 1d). Based on the above

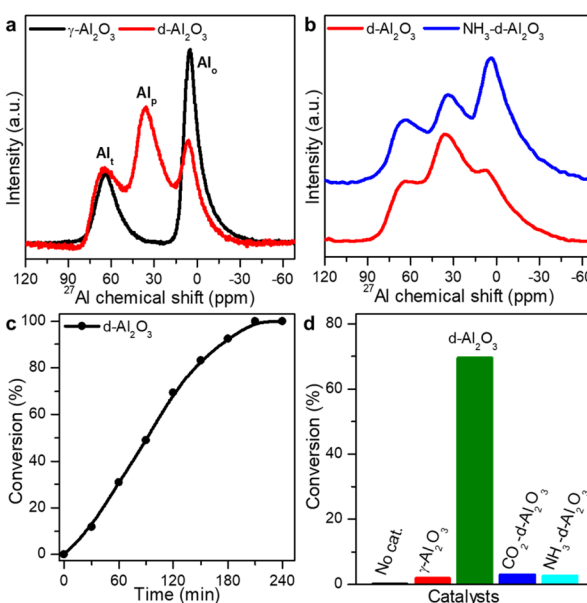


Fig. 1 (a) Solid state ^{27}Al MAS-NMR spectra of γ - Al_2O_3 and d- Al_2O_3 . (b) Solid state ^{27}Al MAS-NMR spectra of d- Al_2O_3 and NH_3 treated d- Al_2O_3 . (c) Catalytic hydrogenation of styrene by d- Al_2O_3 . (d) Catalytic performance comparison of no catalyst, γ - Al_2O_3 , d- Al_2O_3 and d- Al_2O_3 -treated with gaseous Lewis acid or base molecules of CO_2 and NH_3 , respectively. Reaction time: 120 min.



observations, we considered that FLPs were the real active centers for the catalytic hydrogenation of styrene.

2.3 Heterolytic activation of H₂ on FLPs on d-Al₂O₃

The unexpected hydrogenation activity motivated us to deeply understand the H₂ activation and hydrogenation mechanism over the heterogeneous FLPs. The feature of activated hydrogen species on the solid product was first characterized directly by two-dimensional (2D) solid state heteronuclear correlation (HETCOR) NMR spectroscopy.^{42,43} Compared to H₂-treated γ -Al₂O₃, we detected an additionally intense cross peak linking the Al_p site and H ^{δ -} products in H₂-treated d-Al₂O₃ with a short CP contact time (Fig. 2a and S9†). This suggests that H species are adjacent to Al_p sites.⁴⁴ Additionally, we confirmed the existence of Al_p-bonded hydrogen species (Al_p-H ^{δ -}) through *in situ* H₂-FTIR spectroscopy. An obvious peak in the range of 1730–1970 cm⁻¹ confirmed the presence of Al_p-H ^{δ -} in H₂-treated d-Al₂O₃, and abundant O-H ^{δ +} species were observed on the surface of H₂-treated d-Al₂O₃ (Fig. 2b). The above results convincingly revealed that H₂ was activated at the FLP sites *via* the heterolytic activation pathway with the formation of Al_p-H ^{δ -} and O-H ^{δ +}.^{45–48} Furthermore, considering the complicated chemical environment of hydrogen species in the sample,^{49,50} some bound to FLPs while others not, we employed ²H to probe the hydrogen species on the FLPs to exclude other influencing factors.⁵¹ As shown in Fig. 2c (red trace), the solid state ²H MAS-NMR spectra of D₂-treated d-Al₂O₃ showed a peak at 4.2 ppm corresponding to the ²H NMR signal of D₂O (Fig. S10†),⁵² which represented the activated hydrogen species on the FLPs. In contrast to d-Al₂O₃, no ²H signal was detected when γ -Al₂O₃ was

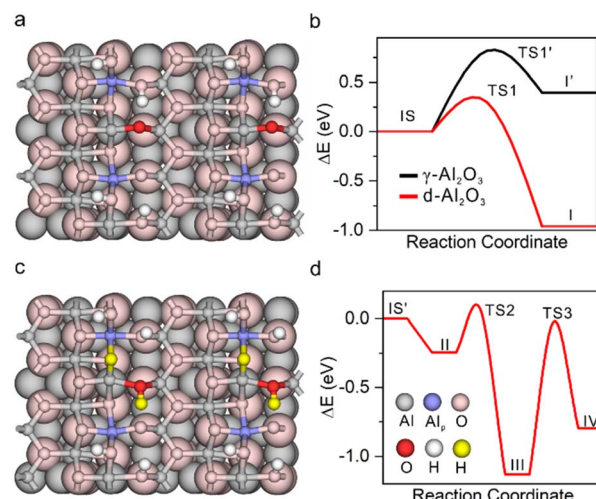


Fig. 3 Structure of (a) d-Al₂O₃ and (c) d-Al₂O₃ with heterolytically dissociated H₂. The colour code is shown in panel (d). Energetic profiles of (b) H₂ activation over γ -Al₂O₃ and d-Al₂O₃, and (d) following stepwise hydrogenation of C₂H₄ over d-Al₂O₃.

treated with D₂ under the same conditions (Fig. 3c, black trace). These results clearly indicate that d-Al₂O₃ with FLPs readily activates H₂, while γ -Al₂O₃ without FLPs did not. Moreover, *in situ* D₂-FTIR spectroscopy demonstrated that d-Al₂O₃ activated D₂ rather than γ -Al₂O₃, as indicated by the distinct signal of the O-D bond during the treatment of d-Al₂O₃ with D₂ (Fig. S11†). The activated hydrogen species (O-H ^{δ +} and Al_p-H ^{δ -}) formed on the FLPs of d-Al₂O₃ reacted readily with styrene. As shown by solid state ²H MAS-NMR, the ²H signal of the deuterated species from the d-Al₂O₃ treated with D₂ disappeared upon the introduction of styrene (Fig. 2c, blue trace). When the d-Al₂O₃ catalyst was treated with D₂ again after the reaction with styrene, the ²H signal reappeared (Fig. 2c, green trace).

DFT calculation was further applied to understand the hydrogenation process.^{53–55} The structure of γ -Al₂O₃ was constructed following the same method in our previous study.⁵⁶ The d-Al₂O₃ model with surface Al_p was constructed from γ -Al₂O₃ following a dehydration process. Considering the high surface concentration of Al_p on the surface of d-Al₂O₃ reported in this work, 1/2 surface hydroxyl group was removed. The resulting coordinatively unsaturated Al_p site and the deprotonated –O⁻ site serve as the FLP center for the H₂ activation and hydrogenation (Fig. 3a). By overcoming a barrier of 0.30 eV (TS1), the heterolytic dissociation of H₂ at the FLP site was exothermic by ~0.96 eV over d-Al₂O₃ (Fig. 3b), resulting in O-H ^{δ +} and Al_p-H ^{δ -} (Fig. 3c). By contrast, the dissociation of H₂ on γ -Al₂O₃ can be only realized on the surface with reconstruction of the surface Al_t with a barrier of 0.82 eV (TS1') and endothermicity of 0.40 eV (Fig. S12†), implying that the activation of H₂ on the pristine γ -Al₂O₃ was restricted. The hydrogenation of ethylene was further calculated to confirm that the heterolytically dissociated hydrogen species were responsible for the catalytic hydrogenation. As shown in Fig. 3d and S13,† the barriers for the stepwise hydride and proton transfer from Al_p-H ^{δ -} and O-H ^{δ +} to

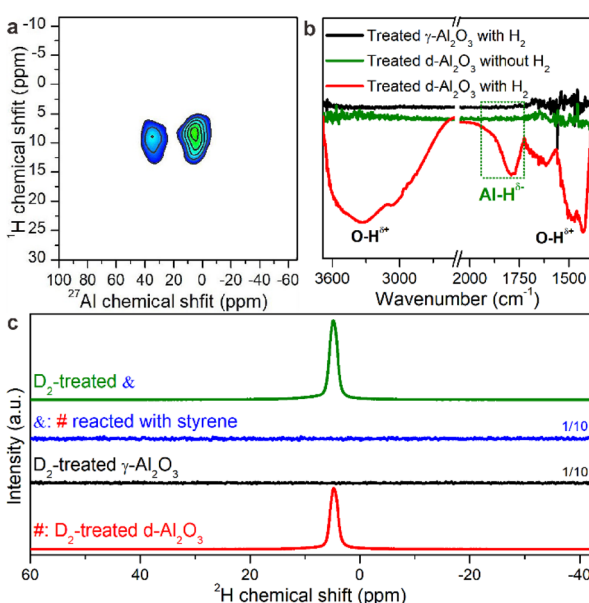


Fig. 2 (a) 2D solid state ¹H-²⁷Al HETCOR spectrum of H₂-treated d-Al₂O₃. (b) *In situ* H₂-FTIR of γ -Al₂O₃, d-Al₂O₃ treated without H₂ and d-Al₂O₃ treated with H₂. (c) Solid state ²H MAS-NMR spectra of D₂-treated d-Al₂O₃ (denoted as #), D₂-treated γ -Al₂O₃, # reacted with styrene (denoted as &), and D₂-treated &.



produce ethane were 0.31 (TS2) and 1.11 eV (TS3), respectively, which was affordable under the catalytic conditions.

2.4 Stepwise hydrogenation mechanism

The catalytic hydrogenation mechanism utilizing $O-H^{\delta+}$ and $Al-H^{\delta-}$ species on FLPs was also verified by isotope-labelling experiments. First, when D_2 -treated $d-Al_2O_3$ was used to react with styrene in anhydrous toluene, the characteristic peaks of deuterated ethylbenzene were observed in 2H NMR spectra (Fig. 4a), indicating that the D_2 dissociated on FLPs of $d-Al_2O_3$ can deuterate styrene and thus verifying the results observed in Fig. 2c. Correspondingly, when D_2 was used as the hydrogen source and D_2 treated $d-Al_2O_3$ as the catalyst, a very strong signal of deuterated ethylbenzene without the presence of other impurities was observed in the 2H NMR spectrum, further confirming that $d-Al_2O_3$ can catalyze hydrogenation of styrene to afford ethylbenzene in $\sim 100\%$ purity (Fig. 4b). Interestingly, we found that the number of D atoms on the alpha carbon atom (C_α) was significantly less than that on the beta carbon atom (C_β). The peak area ratio, $\alpha_D : \beta_D$, was calculated to be 1 : 2.6 (Fig. 4c). The results suggested the existence of the hydrogen–deuterium exchange in the hydrogenation process, which was an indication that the hydrogenation reaction was performed in two steps rather than one step.⁵⁷ As expected, when D_2 and H_2 were used as hydrogen sources respectively, a typical primary kinetic isotope effect (KIE, $k_{H_2}/k_{D_2} > 5$) was observed (Fig. 4d), so the rate-determining step was the cleavage of the O–D bond.^{58,59}

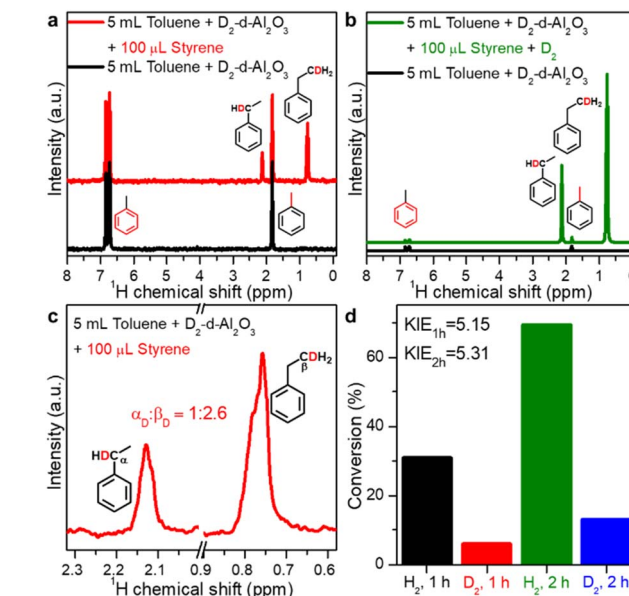


Fig. 4 (a) 2H NMR spectra of toluene mixed with D_2 -treated $d-Al_2O_3$ and D -ethylbenzene from reacting styrene with D_2 -treated $d-Al_2O_3$ in toluene. (b) 2H NMR spectra of toluene mixed with D_2 -treated $d-Al_2O_3$ and D -ethylbenzene from reacting styrene with D_2 and D_2 -treated $d-Al_2O_3$ in toluene. (c) Enlargement of the two peaks of α_D and β_D in Fig. 4a. (d) Primary kinetic isotope effect (PKIE) of styrene hydrogenation.

Based on the above systematic studies, the catalytic pathway of the reaction was proposed (Fig. S14†). The reaction begins with the heterolytic activation of H_2 by FLPs of $d-Al_2O_3$ to produce $O-H^{\delta+}$ and $Al-H^{\delta-}$. Next, the active hydride species react with the adsorbed styrene following an Eley–Rideal-like mechanism, attacking β_C , and then the protons at the O atom interact with α_C . Finally, the obtained ethylbenzene was released and the catalytically active sites were recovered.

2.5 $d-Al_2O_3$ as the catalyst for hydrogenation of other substrates

Furthermore, insight into the mechanism also motivated us to explore the general applicability of the $d-Al_2O_3$ catalyst. Table 1 shows the results of these hydrogenation reactions. First, $d-Al_2O_3$ exhibited nice activity in the hydrogenation of various olefins including aromatic and aliphatic olefins (Table 1, entries 1–4). Moreover, the hydrogenation of aromatic and aliphatic alkynes over $d-Al_2O_3$ gave the corresponding alkanes with excellent yields too (Table 1, entries 5–9). These results strongly suggested that FLPs enabled the

Table 1 Hydrogenation of olefins, alkanes, benzaldehyde and acetophenone catalysed by the $d-Al_2O_3$ catalyst^a

Entry	Substrate	Product	Yield (%)
1 ^b			>99.5
2 ^b			>99.0
3 ^b			>99.9
4 ^b			>99.9
5 ^b			>99.5
6 ^b			>98.5
7 ^b			>99.9
8 ^b			>99.0
9 ^b			>99.5
10 ^c			>98.5
11 ^c			>99.0

^a Reaction conditions: 50 mg $d-Al_2O_3$, 0.2 mmol substrate, 5 mL anhydrous toluene. ^b 100 °C, 8 h, 1 MPa H_2 . ^c 150 °C, 24 h, 4 MPa H_2 .



hydrogenation of both terminal and internal carbon–carbon multiple bonds. Since heterolytic activation of H_2 yielded both $\text{O}-\text{H}^{\delta+}$ and $\text{Al}-\text{H}^{\delta-}$ on the d- Al_2O_3 surface, d- Al_2O_3 should allow the hydrogenation of polar unsaturated bonds.^{60–62} As expected, we observed good catalytic performance in the hydrogenation of benzaldehyde or acetophenone by d- Al_2O_3 (Table 1, entries 10–11).

3 Conclusions

In summary, amorphous Al_2O_3 enriched with surface penta-coordinated Al^{3+} species has been synthesized *via* a simple synthesis method. The co-presence of a large amount of Lewis acidic and basic sites in the same rigid phase thus gave rise to a new type of heterogeneous transition metal-free FLP catalyst. The d- Al_2O_3 catalyst is highly reactive to enable the heterolytic activation of molecular hydrogen. In the hydrogenation of styrene, the FLP-enriched d- Al_2O_3 exhibited nice activity and robustness, and more importantly, a stepwise hydrogenation mechanism. Since heterolytic activation of H_2 yielded both $\text{O}-\text{H}^{\delta+}$ and $\text{Al}-\text{H}^{\delta-}$ on the d- Al_2O_3 surface, d- Al_2O_3 catalyzed the hydrogenation of polar unsaturated bonds in aldehydes or ketones. More work on employing FLP-rich oxides for the discovery of other exciting catalysts should be further explored.

4 Experimental methods

4.1 General procedure for synthesis of d- Al_2O_3

For a typical synthesis process of d- Al_2O_3 , 500 mg $\text{Al}(\text{OH})(\text{CH}_3\text{COO})_2$ was transferred into a glass reaction tube ($\Phi = 1\text{ cm}$). The sample was heated to 500 °C at a rate of temperature increase of 1 °C min⁻¹ for 4 h under N_2 or Ar protection. After cooling to room temperature, the white products were quickly transferred to a dry centrifuge tube, sealed and stored in a desiccator, and used for further characterization.

4.2 General procedure for treatment of d- Al_2O_3 with gaseous Lewis base molecules

For a typical treatment process, d- Al_2O_3 was first synthesized by the above method in a glass reaction tube. After cooling to room temperature, high-purity gases (5 vol% NH_3/Ar) at a rate of 20 mL min⁻¹ were passed with mass flow for 12 h. The products were quickly transferred to a dry centrifuge tube, sealed and stored in a desiccator, as well as used for further characterization. The samples were marked as NH_3 -d- Al_2O_3 .

4.3 General procedure for treatment of d- Al_2O_3 with H_2 or D_2

For a typical treatment process, d- Al_2O_3 was first synthesized by the above method in a glass reaction tube. After cooling to room temperature, the sample was heated to 100 °C at a rate of temperature increase of 1 °C min⁻¹ for 2 h under H_2 or D_2 protection. After cooling to room temperature, the products were quickly transferred to a dry centrifuge tube, sealed and stored in a desiccator, which was used for further characterization and applications.

4.4 General procedure for catalysis tests

For a typical styrene hydrogenation reaction, a freshly prepared 50 mg catalyst of d- Al_2O_3 was dispersed in 5 mL anhydrous toluene, and then 20 μL styrene was added in an autoclave under stirring. Next, the reactor was charged with H_2 to 1 MPa and kept at 100 °C in an oil bath during stirring. The products were analyzed by gas chromatography (GC9720Plus, Fuli Instruments) for conversion determination. For other catalysts, the reaction conditions were the same as above. In the catalyst recycling test, after the first cycle was carried out for 150 min, the same amount of styrene was added to the reactor and the reaction was allowed to take place. As mentioned above, the recycling was repeated another six times.

4.5 Solid state ^{27}Al MAS NMR characterization

Solid state ^{27}Al MAS-NMR measurement (Fig. 1a) was performed using a Bruker Avance NEO 600 MHz spectrometer with a 3.2 mm probe head at a spinning rate of 20 kHz. Spectra were accumulated for 1000 scans with a cycle delay of 2.5 s, using a pulse width of $\pi/6$. Solid state ^{27}Al MAS-NMR measurement (Fig. 1b) was performed using a Bruker Avance III 400 MHz spectrometer with a 4.0 mm probe head at a spinning rate of 12 kHz. Spectra were accumulated for 256 scans with a recycle delay of 2 s and a pulse width of $\pi/2$ was used. It is worth noting that the magnetic field strength and pulse width hardly affected the relative content of Al^{3+} ions in the different coordination environments in our test. The fitting of ^{27}Al NMR spectra was conducted using the Dmfit program, which includes the quadrupolar interactions for ^{27}Al MAS NMR. The CzSimple model was applied for the fitting, which implements a rapid version of the Czjzek distribution of quadrupolar interaction. The Gaussian isotropic model for $d = 5$ with an uncoupled distribution of isotropic chemical shift was included in the simulations. All the other parameters were freely variable during the fitting.⁶³

4.6 2D solid state ^1H – ^{27}Al heteronuclear correlation (HETCOR) experiment

The experiment was performed on a Bruker Avance NEO 600 MHz spectrometer with a 3.2 mm probe head under MAS conditions of 15 kHz with a very short CP contact time of 50 μs .

4.7 Solid state ^2H MAS NMR characterization

Solid state ^2H MAS NMR spectra were recorded on a Bruker Avance III NEO 600 MHz spectrometer with a 3.2 mm probe head at a spinning rate of 15 kHz, and the spectra were accumulated for 1024 scans with a cycle delay of 1 s, and a pulse width of $\pi/2$ was used.

4.8 Liquid state ^1H NMR characterization

^1H NMR spectra were recorded on an AVANCE III 500 MHz spectrometer.



4.9 Liquid state ^2H NMR characterization

^2H NMR spectra were recorded on an AVANCE III 850 MHz spectrometer. All NMR data were processed on MestReNova software.

4.10 *In situ* diffuse reflectance FTIR characterization

Typically, d-Al₂O₃ was first synthesized in an *in situ* chamber of FTIR (Thermo Fisher IS50) at 500 °C under Ar protection, and the sample was cooled to 30 °C to acquire background. For *in situ* NH₃-FTIR, 5 vol% NH₃/Ar was charged into the chamber at a rate of 30 mL min⁻¹ while pure Ar was turned off, and spectra were collected until stable adsorption with NH₃. *In situ* CO₂-FTIR spectra were recorded in the same way. *In situ* D₂-FTIR spectra were recorded in the same way except that the test temperature is 100 °C.

4.11 TPD-MS characterization

Typically, NH₃-TPD-MS was performed on a Micromeritics AutoChem II 2920 instrument equipped with a mass spectrometer. The 100 mg d-Al₂O₃ sample was first synthesized at 500 °C under Ar protection. The sample was then cooled to room temperature and treated under 5 vol% NH₃/He gas flow for 30 min. The gaseous and weakly adsorbed NH₃ was subsequently removed by purging with He for 60 min. Subsequently, the temperature was raised from room temperature to 700 °C at a rate of 10 °C min⁻¹ and the NH₃-TPD profile was recorded by using a mass spectrometer with a signal of *m/z* = 16. For CO₂-TPD-MS, 5 vol% CO₂/He gas was used, and the CO₂-TPD profile was recorded by using a mass spectrometer with a signal of *m/z* = 44.

4.12 N₂ adsorption/desorption characterization

N₂ adsorption/desorption measurements were conducted on a Micromeritics ASAP 2020 gas adsorption analyzer. The freshly prepared sample was first degassed at 300 °C for 8 h. Then, the specific surface areas were determined using the Brunauer-Emmett-Teller (BET) and Langmuir equations from the N₂ sorption data.

4.13 XRD characterization

X-ray powder diffraction experiments were conducted on a Rigaku Ultima IV using Cu K α radiation. The operation voltage and current were 40 kV and 30 mA, respectively. The scanning speed was set to be 15 ° min⁻¹.

4.14 HAADF-STEM characterization

High-angle annular-dark-field (HAADF) images were acquired using a JEOL 200F transmission electron microscope operated at 200 keV. The attainable spatial resolution of the microscope was 78 pm with a probe spherical-aberration corrector. Images were acquired with the illumination semi-angle of 25 mrad and probe current of 100 pA. The dwell time for image acquisition was set at 10 microseconds per pixel to ensure a desirable signal-to-noise ratio.

4.15 Computational details

The spin-polarized density functional theory (DFT) calculations were performed using the Vienna *ab initio* simulation package (VASP5.4.4).⁶⁴⁻⁶⁷ The core electrons were replaced by the projector augmented wave (PAW) pseudopotentials,^{65,68} and the valence electrons were described by a plane wave basis set with a cut-off energy of 400 eV. The electron exchange and correlation were treated by Perdew-Burke-Ernzerhof (PBE) generalized gradient approximation (GGA).⁶⁹ The *k*-point sampling was generated by following the Monkhorst-Pack procedure with a 3 × 3 × 1 mesh.⁷⁰ The transition states (TSs) were determined using the nudged elastic band (NEB) approach. The TS structures were optimized using a quasi-Newton algorithm. The steady states and TSs were converged to a residual force smaller than 0.03 eV Å⁻¹ and 0.05 eV Å⁻¹, respectively. All the minima and TSs were confirmed by the vibrational frequency calculations. The reaction barrier was defined as $\Delta E_a = E_{\text{TS}} - E_{\text{R}}$, where E_R and E_{TS} were the energies of the reactant on the slab and the corresponding transition states, respectively.

Data availability

All the data supporting this article have been included in ESI.†

Author contributions

N. F. Z. conceived and supervised the research project. Q. Y. W. synthesized and characterized the samples, as well as investigated the catalytic performances and mechanism. R. X. Q. performed DFT calculations. M. S. Z., Y. Y. Z and S. S. Y. contributed to the NMR and TPD measurements. G. F. provided some suggestions. N. F. Z., and Q. Y. W. wrote and revised the manuscript. X. D. Y and H. S. revised the manuscript.

Conflicts of interest

The authors declare no competing financial interests.

Acknowledgements

We acknowledge financial support from the National Natural Science Foundation of China (grant no. 92261207, 22202164, and NSFC Center for Single-Atom Catalysis under grant no. 22388102) and the New Cornerstone Science Foundation. Q. Y. W. thanks the China Postdoctoral Science Foundation Project (2023M732946). R. X. Q. acknowledges support from National Key R&D Program of China (2022YFA1504500), the Natural Science Foundation of Fujian Province (2023J05006) and the Fundamental Research Funds for the Central Universities (20720230002). We also thank Prof. Lin Gu and Dr Qinghua Zhang at the Institute of Physics of the Chinese Academy of Sciences for the TEM measurements.

References

- 1 G. S. McGrady and G. Guilera, *Chem. Soc. Rev.*, 2003, **32**, 383.
- 2 G. J. Kubas, *Acc. Chem. Res.*, 1988, **21**, 120.

3 D. M. Heinekey, A. Lledos and J. M. Lluch, *Chem. Soc. Rev.*, 2004, **33**, 175.

4 P. G. Jessop and R. H. Morris, *Coord. Chem. Rev.*, 1992, **121**, 155.

5 A. I. Krasna and D. Rittenberg, *J. Am. Chem. Soc.*, 1954, **76**, 3015.

6 D. Schilter, J. M. Camara, M. T. Huynh, S. S. Hammes and T. B. Rauchfuss, *Chem. Rev.*, 2016, **116**, 8693.

7 W. Lubitz, H. Ogata, O. Rudiger and E. Reijerse, *Chem. Rev.*, 2014, **114**, 4081.

8 S. Aldridge and A. J. Downs, *Chem. Rev.*, 2001, **101**, 3305.

9 G. C. Welch, R. R. San Juan, J. D. Masuda and D. W. Stephan, *Science*, 2006, **314**, 1124.

10 P. Spies, G. Erker, G. Kehr, K. Bergander, R. Frohlich, S. Grimme and D. W. Stephan, *Chem. Commun.*, 2007, 5072.

11 G. C. Welch and D. W. Stephan, *J. Am. Chem. Soc.*, 2007, **129**, 1880.

12 P. A. Chase, G. C. Welch, T. Jurca and D. W. Stephan, *Angew. Chem., Int. Ed.*, 2007, **119**, 8196.

13 G. C. Welch, L. Cabrera, P. A. Chase, E. Hollink, J. D. Masuda, P. Wei and D. W. Stephan, *Dalton Trans.*, 2007, 3407.

14 D. W. Stephan, *Science*, 2016, **354**, aaf7229.

15 D. W. Stephan and G. Erker, *Angew. Chem., Int. Ed.*, 2010, **49**, 46.

16 D. W. Stephan, *Acc. Chem. Res.*, 2015, **48**, 306.

17 Y. Ma, S. Zhang, C. Chang, Z. Huang, J. Ho and Y. Qu, *Chem. Soc. Rev.*, 2018, **47**, 5541.

18 G. Lu, P. Zhang, D. Sun, L. Wang, K. Zhou, Z. Wang and G. Guo, *Chem. Sci.*, 2014, **5**, 1082.

19 K. C. Szeto, W. Sahyoun, N. Merle, J. L. Castelbou, N. Popoff, F. Lefebvre, J. Raynaud, C. Godard, C. Claver, L. Delevoye, R. M. Gauvin and M. Taoufik, *Catal. Sci. Technol.*, 2016, **6**, 882.

20 J. Y. Xing, J. C. Buffet, N. H. Rees, P. Norby and D. O'Hare, *Chem. Commun.*, 2016, **52**, 10478.

21 K. K. Ghuman, T. E. Wood, L. B. Hoch, C. A. Mims, G. A. Ozin and C. V. Singh, *Phys. Chem. Chem. Phys.*, 2015, **17**, 14623.

22 K. K. Ghuman, L. B. Hoch, P. Szymanski, J. Y. Y. Loh, N. P. Kherani, M. A. El-Sayed, G. A. Ozin and C. V. Singh, *J. Am. Chem. Soc.*, 2016, **138**, 1206.

23 L. He, T. E. Wood, B. Wu, Y. Dong, L. B. Hoch, L. M. Reyes, D. Wang, C. Kübel, C. Qian, J. Jia, K. Liao, P. G. O'Brien, A. Sandhel, J. Y. Y. Loh, P. Szymanski, N. P. Kherani, T. C. Sum, C. A. Mims and G. A. Ozin, *ACS Nano*, 2016, **10**, 5578.

24 L. B. Hoch, L. He, Q. Qiao, K. Liao, L. M. Reyes, Y. Zhu and G. A. Ozin, *Chem. Mater.*, 2016, **28**, 4160.

25 A. Primo, F. Neatu, M. Florea, V. Parvulescu and H. Garcia, *Nat. Commun.*, 2014, 5291.

26 J. Zhao, X. Liu and Z. Chen, *ACS Catal.*, 2017, **7**, 766.

27 X. Zhao, J. Wang, M. Yang, N. Lei, L. Li, B. Hou, S. Miao, X. Pan, A. Wang and T. Zhang, *ChemSusChem*, 2017, **10**, 819.

28 H. Lee, Y. N. Choi, D. W. Lim, M. M. Rahman, Y. I. Kim, I. H. Cho, H. W. Kang, J. H. Seo, C. Jeon and K. B. Yoon, *Angew. Chem., Int. Ed.*, 2015, **54**, 13080.

29 T. Mahdi and D. W. Stephan, *Angew. Chem., Int. Ed.*, 2015, **54**, 8511.

30 M. Trunk, J. F. Teichert and A. Thomas, *J. Am. Chem. Soc.*, 2017, **139**, 3615.

31 S. Zhang, Z. Huang, Y. Ma, W. Gao, J. Li, F. Cao, L. Li, C. Chang and Y. Qu, *Nat. Commun.*, 2017, **8**, 15266.

32 S. G. Hindin and S. W. Weller, *J. Phys. Chem.*, 1956, **60**, 1501.

33 Y. Amenomiya, J. H. B. Chenier and R. J. Cvetanovic, *J. Catal.*, 1967, **9**, 28.

34 J. H. Kwak, J. Hu, D. Mei, C. W. Yi, D. H. Kim, C. H. Peden, L. F. Allard and J. Szanyi, *Science*, 2009, **325**, 1670.

35 N. Tang, Y. Cong, Q. Shang, C. Wu, G. Xu and X. Wang, *ACS Catal.*, 2017, **7**, 5987.

36 Z. Zhang, Y. Zhu, H. Asakura, B. Zhang, J. Zhang, M. Zhou, Y. Han, T. Tanaka, A. Wang, T. Zhang and N. Yan, *Nat. Commun.*, 2017, **8**, 16100.

37 P. Liu, R. Qin, G. Fu and N. F. Zheng, *J. Am. Chem. Soc.*, 2017, **139**, 2122.

38 Q. Wu, R. Qin, D. Zang, W. Zhang, B. Wu and N. F. Zheng, *Acta Chim. Sin.*, 2018, **76**, 617.

39 R. Qin, K. Liu, Q. Wu and N. F. Zheng, *Chem. Rev.*, 2020, **120**, 11810.

40 Q. Wu, W. Zhou, H. Shen, R. Qin, Q. Hong, X. Yi and N. Zheng, *CCS Chem.*, 2023, **5**, 1215.

41 L. Shi, G. M. Deng, W. C. Li, S. Miao, Q. N. Wang, W. P. Zhang and A. H. Lu, *Angew. Chem., Int. Ed.*, 2015, **54**, 13994.

42 S. h. Xin, Q. Wang, J. Xu, N. D. Feng, W. Z. Li and F. Deng, *Solid State Nucl. Magn. Reson.*, 2017, **84**, 103.

43 L. Wang, G. Kehr, C. G. Daniliuc, M. Brinkkötter, T. Wiegand, A.-L. Wübker, H. Eckert, L. Liu, J. G. Brandenburg, S. Grimme and G. Erker, *Chem. Sci.*, 2018, **9**, 4859.

44 K. R. Graham, C. Cabanetos, J. P. Jahnke, M. N. Idso, A. El Labban, G. O. Ngongang Ndjawa, T. Heumueller, K. Vandewal, A. Salleo, B. F. Chmelka, A. Amassian, P. M. Beaujuge and M. D. McGehee, *J. Am. Chem. Soc.*, 2014, **136**, 9608.

45 B. Werghi, A. Bendjeriou-Sedjerari, A. Jedidi, E. Abou-Hamad, L. Cavallo and J. M. Basset, *Organometallics*, 2016, **35**, 3288.

46 M. Veith, J. Frères, V. Huch and M. Zimmer, *Organometallics*, 2006, **25**, 1875.

47 R. Wischert, C. Coperet, F. Delbecq and P. Sautet, *Angew. Chem., Int. Ed.*, 2011, **123**, 3260.

48 J. Joubert, A. Salameh, V. Krakoviack, F. Delbecq, P. Sautet, C. Copéret and J. M. Basset, *J. Phys. Chem. B*, 2006, **110**, 23944.

49 H. Shen, Q. Wu, M. S. Asre Hazer, X. Tang, Y.-Z. Han, R. Qin, C. Ma, S. Malola, B. K. Teo, H. Häkkinen and N. Zheng, *Chem.*, 2022, **8**, 2380.

50 H. Shen, Q. Wu, S. Malola, Y.-Z. Han, Z. Xu, R. Qin, X. Tang, Y.-B. Chen, B. K. Teo, H. Häkkinen and N. Zheng, *J. Am. Chem. Soc.*, 2022, **144**, 10844.

51 C. Sun, N. Mammen, S. Kaappa, P. Yuan, G. Deng, C. Zhao, J. Yan, S. Malola, K. Honkala, H. Häkkinen, B. K. Teo and N. Zheng, *ACS Nano*, 2019, **13**, 5975.



52 T. Mizuno, T. Nemoto, M. Tansho, T. Shimizu, H. Ishii and K. Takegoshi, *J. Am. Chem. Soc.*, 2006, **128**, 9683.

53 W. Zhang, R. Qin, G. Fu and N. Zheng, *J. Am. Chem. Soc.*, 2023, **145**, 10178.

54 K. Li, R. Qin, K. Liu, W. Zhou, N. Liu, Y. Zhang, S. Liu, J. Chen, G. Fu and N. Zheng, *ACS Appl. Mater. Interfaces*, 2021, **13**, 52193.

55 W. Zhang, R. Qin, G. Fu and N. Zheng, *J. Am. Chem. Soc.*, 2021, **143**, 15882.

56 R. Qin, L. Zhou, P. Liu, Y. Gong, K. Liu, C. Xu, Y. Zhao, L. Gu, G. Fu and N. F. Zheng, *Nat. Catal.*, 2020, **3**, 703.

57 P. Liu, Y. Zhao, R. Qin, S. Mo, G. Chen, L. Gu, D. M. Chevrier, P. Zhang, Q. Guo, D. Zang, B. Wu, G. Fu and N. F. Zheng, *Science*, 2016, **352**, 797.

58 K. Liu, R. Qin, L. Zhou, P. Liu, Q. Zhang, W. Jing, P. Ruan, L. Gu, G. Fu and N. Zheng, *CCS Chem.*, 2019, **1**, 207.

59 C. Xu, G. Chen, Y. Zhao, P. Liu, X. Duan, L. Gu, G. Fu, Y. Yuan and N. Zheng, *Nat. Commun.*, 2018, **9**, 3367.

60 A. Comas-Vives, C. González-Arellano, A. Corma, M. Iglesias, F. Sánchez and G. Ujaque, *J. Am. Chem. Soc.*, 2006, **128**, 4756.

61 P. Liu, Y. Zhao, R. Qin, S. Mo, G. Chen, L. Gu, D. M. Chevrier, P. Zhang, Q. Guo, D. Zang, B. Wu, G. Fu and N. Zheng, *Science*, 2016, **352**, 797.

62 A. Dedieu, S. Humbel, C. Elsevier and C. Grauffel, *Theor. Chem. Acc.*, 2004, **112**, 305.

63 D. Massiot, F. Fayon, M. Capron, I. King, S. Le Calvé, B. Alonso, J.-O. Durand, B. Bujoli, Z. Gan and G. Hoatson, *Magn. Reson. Chem.*, 2002, **40**, 70.

64 G. Kresse and J. Hafner, *Phys. Rev. B*, 1994, **49**, 14251.

65 G. Kresse and J. Hafner, *Phys. Rev. B*, 1993, **48**, 13115.

66 G. Kresse and J. Furthmüller, *Comput. Mater. Sci.*, 1996, **6**, 15.

67 G. Kresse and J. Furthmüller, *Phys. Rev. B*, 1996, **54**, 11169.

68 G. Kresse and D. Joubert, *Phys. Rev. B*, 1999, **59**, 1758.

69 G. Kresse and J. Hafner, *Phys. Rev. B*, 1993, **47**, 558.

70 H. J. Monkhorst and J. D. Pack, *Phys. Rev. B*, 1976, **13**, 5188.

